ESOGÜ Müh Mim Fak Derg. 2022, 30(3), 397-404 J ESOGU Engin Arch Fac. 2022, 30(3), 397-404

PERFORMANCE COMPARISON OF PARALLEL AND SERIES CHANNEL COLD PLATES USED IN ELECTRIC VEHICLES BY MEANS OF CFD SIMULATIONS

Ayhan Nazmi İLİKAN[1*], Ahmet YAYLI[2]

[1] TÜBİTAK RUTE, Kocaeli, ORCID No : http://orcid.org/0000-0001-9497-2406
[2] TÜBİTAK RUTE, Kocaeli, ORCID No : http://orcid.org/0000-0003-4404-5609

Keywords

Cold plate
Li-ion battery
CFD
Thermal resistance
Pressure drop

Abstract

In a cold plate low thermal resistance thus high heat transfer rate and also low pressure drop is desired. In this study, performances of three liquid cold plates with different configurations are investigated for the thermal regulation of li-ion battery cells in electric vehicle applications. The outer dimensions of the cold plates are kept identical in order to use the cold plates in the same battery module under series, parallel and series-parallel configurations. The performances of the cold plates are investigated by using Computational Fluid Dynamic (CFD) tools. ANSYS Fluent commercial software is used to calculate the flow field and the thermal field inside the cold plates for various flowrates. The performances of the cold plates are obtained by 3D simulations that solve Navier-Stokes, energy and continuity equations in a steady manner. The flow is assumed to be laminar for all the cases since calculated Reynolds number stay in laminar flow limits. The results show that the pressure drop of the coolant liquid of parallel flow arrangement is significantly lower than the serial arrangement. However, high thermal resistance and low uniformity of the temperature through the cold plate is observed compared to the serial case, as expected. As a result, series-parallel configuration results show that the trade-off between pressure drop and heat transfer rate can be optimized by applying a serpentine shape while keeping the flow arrangement as parallel as possible and increasing the length of the cross channels.

ELEKTRİKLİ ARAÇLARDA KULLANILAN PARALEL VE SERİ KANALLI SOĞUTMA PLAKALARININ PERFORMANSLARININ HAD YÖNTEMİ İLE KARŞILAŞTIRILMASI

Anahtar Kelimeler

Soğutucu levha
Li-iyon batarya
HAD
Termal direnç
Basınç kaybı

Öz

Soğutucu levhalarda düşük ısıl direnç, dolayısıyla yüksek ısı transferi ve düşük basınç kaybı arzu edilmektedir. Bu çalışmada, elektrikli araç uygulamalarında li-iyon pil hücrelerinin termal regülasyonu için, farklı konfigürasyonlara sahip sıvı soğutmalı üç soğutucu levhanın performansları incelenmiştir. Seri, paralel ve seri-paralel konfigürasyonlarda oluşturulan soğutucu levhaların aynı batarya modülünde kullanılabilmeleri için dış boyutları birbiriyle aynı tutulmuştur. Soğuk plakaların performansları, HAD araçları kullanılarak incelenmiştir. Çeşitli akış hızlarında, soğuk plakaların içindeki akış alanını ve termal alanı hesaplamak için ANSYS Fluent ticari yazılımı kullanılmıştır. Soğuk plakaların performansları, sürekli rejimde Navier-Stokes, enerji ve süreklilik denklemleri 3 boyutlu simülasyonlar ile çözülerek elde edilmiştir. Reynolds sayısı laminer akış limitleri içerisinde hesaplandığından, tüm akış durumları için laminer akış seçilerek çözülmüştür. Simülasyonlar sonucunda, paralel akış geometrisindeki soğutucu sıvının basınç kaybının seri olana göre önemli ölçüde daha düşük olduğu görülmüş, beklenildiği gibi, paralel akış geometrisinde seriye göre yüksek ısıl direnç ve düşük sıcaklık homojenliği gözlemlenmiştir. Sonuç olarak, basınç düşüşü ve ısı transferi arasındaki dengenin, akış düzeninin mümkün olduğunca paralel tutulup çapraz kanalların ise uzunluğunun arttırıldığı bir serpantin şekli uygulanarak optimize edilebileceğini seri-paralel konfigürasyon sonuçları göstermektedir.

[*] Sorumlu yazar; e-posta : ayhan.ilikan@tubitak.gov.tr

Araştırma Makalesi		Research Article	
Başvuru Tarihi	: 21.06.2022	Submission Date	: 21.06.2022
Kabul Tarihi	: 16.09.2022	Accepted Date	: 16.09.2022

1. Introduction

Number of electric vehicles on roads is continuously increasing as a result of developments in battery technology. In the last decade, specific power and specific energy of battery cells have been increased significantly due to advancements in cell chemistries. Typically, these high power and high energy battery cells can withstand approximately 3C for continuous operation and 10C for short term working conditions (Jung, Jang, Hassoun, Sun and Scrosati, 2011), where 1C rate denotes nominal discharge/charge current that a battery cell is exposed to. Resistive heat generation during charge/discharge is known to be approximately proportional to the square of current applied (Schöner and Ogborn, 1987). Thus, high current rates require robust cooling system that can dissipate generated heat and keep battery cells at safe temperature levels. Besides, uniform temperature distribution among battery cells is another must to keep battery packs safe and to extend lifetime of cells. To do so, a maximum temperature difference of 3-5° C is frequently used as a design criterion in battery cooling applications (Dincer, Hamut and Javani, 2017; Warner, 2015). Electric vehicle battery packs usually consist of several battery modules that can be interchanged easily in case of malfunction or failure. These modules typically consist of 4-20 battery cells. In early electric vehicle applications, air cooling were used whereas it is rapidly being replaced by liquid cooling due to aforementioned high capacity cooling demands. As an example, a comparative CFD study conducted by Chen, Jiang, Yang and Pesaran (2016) shows that air cooling requires considerably more parasitic power than liquid cooling to keep the same average temperature of the same module under same operating conditions. A common application to increase heat transfer is to place liquid cold plate on one of the surfaces of battery modules and connect it to thin aluminum plates (cooling fin) situated between the battery cells. In that case, the liquid does not circulate through the thin plates. Thus, generated heat is transferred to the cold plate medium via conduction first, from the cell to the thin plate, then to the cold plate material and finally to the liquid. On the other hand, there are some examples that can provide more effective cooling by circulating the cooling liquid through the thin plates as well. However, this time complexity of the design increases that may bring potential leakage problems. In an experimental study conducted by Teng and Yeow (2012), two liquid cooling systems for electric vehicles, one with thin plates and one with liquid filled microchannels, are designed and compared to each other. They determined that the one with microchannels has several advantages such as more uniform temperature distribution and possibility better cooled cell terminals if the microchannels are optimized for a particular cell. However, the drawback is indicated to be considerably higher cost for a low production volume. Teng, Ma, Yeow and Thelliez (2011) also studied air cooling and reported that if no plate is used and direct air cooling is applied, worse temperature uniformity is achieved since in cold plate case, the heat absorbed by the plate is easily distributed through the plate that can help redistribution of the temperature on the cell surface. Another possibility to provide uniform temperature distribution while keeping maximum temperature at low levels is to use dual cold plates. Yeow, Teng, Thelliez and Tan (2012) performed simulations by using both single and dual cold plates and stated that dual plate can be used for busbar and terminal cooling. Panchal, Mathewson, Fraser, Culham and Fowler (2015) claims non-uniform temperature distribution in spite of using dual cold plates with microchannels filled with liquid. Yeow and Teng (2013) experimented with new materials instead of thin aluminum plates between cells such as thermal pyrolytic graphite materials. This material is reported to have significantly higher conductivity than aluminum for the same density which results in much more uniform temperature distribution with lower temperature on cell surfaces.

The above-mentioned studies incorporate a wide range of cooling systems. If liquid cooling is chosen, whether thin plates between battery cells have microchannels or not, one of the major factors that influence cooling system performance is flow structure within cold plate. A low thermal resistance with low pressure drop cold plate is desired for maximum heat transfer with low external energy. Virtually infinite possible flow configurations can be designed, but in principle, series or parallel flow configurations are studied in open literature by taking channel cross section, shape, length etc. as working parameters (Datta and Majumdar, 1980; Solowitz and Mainka, 2011; Haifeng, Ze-Chang, Xuezhe and Shugiang, 2015; Jarret, 2011; Kandlikar and Hayner, 2009; Rahman, Rahman, Mahlia, and Sheng, 2016).

This study deals with the comparison of thermal and pressure drop performances of three liquid cold plates designed for an electric vehicle battery module. The battery modules' outer dimensions are fixed by design criteria and thus height, width and depth of the liquid cold plate remain constant. Total heat generated by cells inside the module for severe working conditions is applied as a boundary condition to the top surface of the cold plates for all the simulations. One series, one parallel and one series-parallel flow configurations through the liquid cold plate are designed. Detailed analyses are performed for design flowrate and the simulations are extended to higher and lower flowrates to obtain full performance charts that would enable parametric studies.

2. Numerical Procedure

Numerical procedure consists of geometry creation, mesh creation, grid independency tests, preprocess and application of boundary conditions, solution process and post-process phases. Detailed information is provided in the following subsections of this paper.

2.1 Geometry creation

Cold plates are designed to keep li-ion battery cells in effective but safe temperature levels. Optimum temperature range of li-ion battery cells are stated between 15-35° C (Khan, Swierczynski and Kaer, 2017). Thus, cooling capacity of a cold plate geometry is vital for performance, cycle-life and safety of battery cells. In this study, a parallel flow configuration within the cold plate is considered as a baseline and several geometry changes has been made in order to obtain temperature distribution on the top surface (the surface adjacent to the heat source) as uniform as possible. These geometry modifications include the contraction and the expansion angles of the manifolds within the cold plate. Furthermore, the number and the width of the channels perpendicular to the manifolds are also modified for the same purpose. Finally, the geometry shown in Fig. 1, namely "Parallel" is obtained. Another well-known candidate is a "Series" channel configuration. This time, channel width is kept constant from inlet to outlet that is narrower compared to the parallel case. The reason of decreasing the width compared to the "Parallel" channel case is related to number of cycles of the channel within the cold plate that would be insufficient if the width of the channel was kept the same as the first "Parallel" case. Finally, a combination of series and parallel configuration shown again in Fig. 1 is a developed version of the perpendicular channels in "Parallel" case. These channels do not traverse directly to the exit manifold, but make small cycles as in "Series" configuration case.

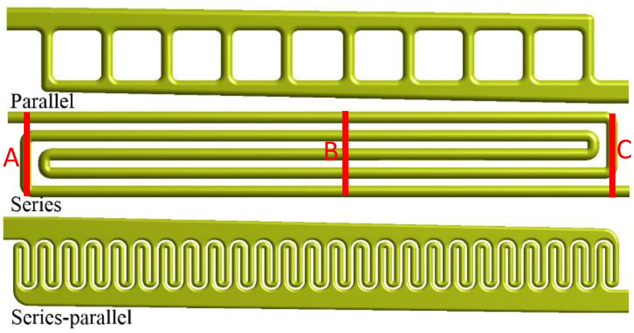

Figure 1. Designed geometries

2.2 Mesh creation and grid independency

The computational grid is created by using ANSYS Mesh; cutcell method supported by ANSYS Fluent is applied to obtain high quality hexahedral elements that enables better convergence characteristics. Besides, the cells can be generated rather rapidly using this method (ANSYS, 2011). A grid independency test is performed to make the solution independent of the cell size. The variation of the maximum temperature on the top surface of the cold plate in function of the total number of mesh elements is shown in Fig. 2.

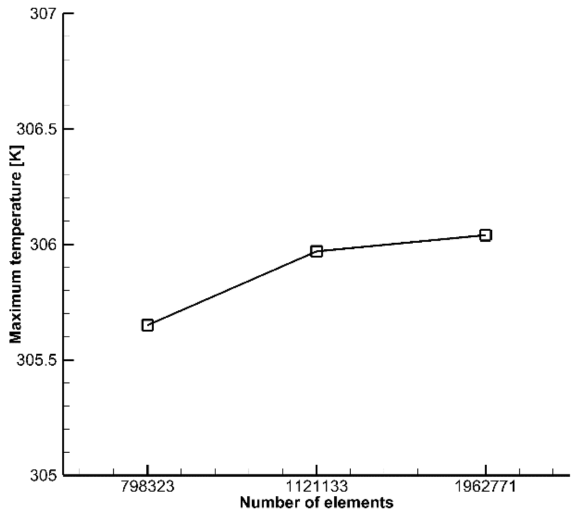

a)

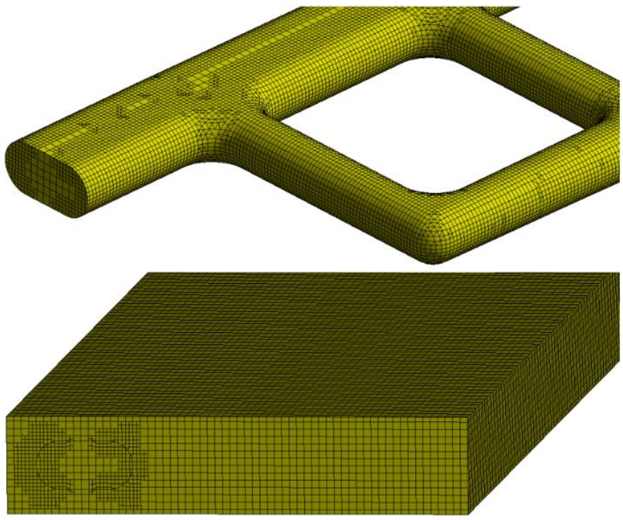

b)

Figure 2. Grid independency study results: a) Maximum temperature variation, b) Generated mesh

Figure 2a shows that no significant change of maximum temperature can be seen from second grid to the third one. Thus, the grid with 1121133 elements is used for the rest of the calculations. The mesh created in that case is shown in Fig. 2b.

2.3 Simulation setup

The geometry consists of two volumes. The solid volume represents the aluminum cold plate block and the fluid volume represents the fluid circulating within the internal channels inside the block. All the simulations are performed for 3D and steady conditions by using commercial finite volume solver ANSYS Fluent. Water at 20°C is applied at the inlet of the cold plates as the working fluid. The calculation of the Reynolds number is based on the hydraulic diameter calculated by using both the inlet of the pipe and the micro channel diameter show that the flow is laminar. Thus, no turbulence model is needed to be used during any calculations. The governing equations are solved by pressure based coupled solver with double precision provided by the code. Second order upwind spatial discretization scheme is used to obtain the solutions of all the equations. Convergence criteria is set as 10^{-5} for the residuals of all the transport equations. For all the three cases, the simulations are performed by applying exactly the same boundary and solver configurations.

2.4 Boundary conditions

The names of the fluid and the solid surfaces and the corresponding boundary conditions are shown in Fig. 3 and Table 1, respectively. For all the simulations, the gauge pressure at the outlet of the channel is set as 0 Pa but the mass flow at the inlet of the channel is varied to obtain the performances of the cold plates at different flowrates.

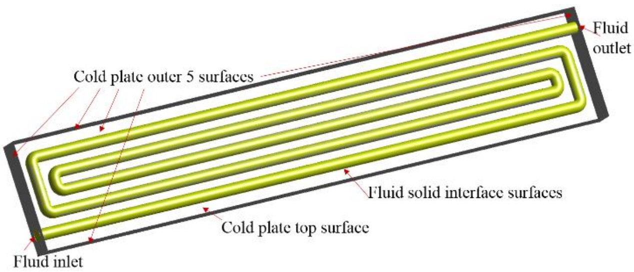

Figure 3. Boundary surfaces

On the other hand, the temperature of the fluid at the inlet is kept as 293 K for all the simulations. The interfaces that allows heat to pass between the fluid and the solid volumes are generated automatically by the code. The top surface of the cold plate is considered as the surface that absorbs heat created by the battery cells inside the module. Thus, a constant heat rate value of 100 W-considered as the maximum heat generated during the maximum permitted current flows through the cell- is distributed uniformly to that surface as a heat flux. This value is chosen by estimating the total heat generated by the cells inside the module. 3C continuous discharge is assumed to be the design condition and the module is designed to have 2 cold plates that means total heat generated inside the module is 200 W. In the end, the rate of the heat that should be absorbed from one cold plate is calculated as 100 W. The other five outer surfaces of the cold plate are considered as insulated since the cold plate is covered by the casing of the module that may prevent the heat to be dissipated to the environment. The authors declare that research and publication ethics were followed in this study.

Table 1
Boundary Surfaces

Boundary Surface	Boundary Condition
Fluid Inlet	Mass flow inlet
Fluıd Outlet	Pressure outlet
Fluid-solid interface surfaces	Coupled wall
Cold plate top surface	Uniform heat flux
Cold plate other outer surfaces	Adiabatic

3. Results and Discussion

The simulations for all the three configurations are performed for several flowrates that help to build performance charts shown at the end of the following subsections. The detailed analysis of the flowfield and temperature field are only investigated for the design flowrate that is 0.0036 kg/s which corresponds approximately to 0.2 L/min.

3.1 Flowfield investigation

The flowfield corresponding to the three configurations obtained at a midsection of the cold plate for the design flowrate are shown in Fig. 4. The pressure contours show that the order of magnitude corresponding to the pressure loss is the same for parallel and series-parallel cases, while the series case has a 25 times larger pressure loss. This is an expected phenomenon since sum of pressure losses for parallel channels are counted as the same regardless of the number of the channels; that is already known from Bernoulli's principle. On the other hand, the width of the channel of the series configuration is narrower that causes higher velocity within the channel for the same flowrate. Again, it is known that pressure drop is directly proportional to the square of the velocity that is the first cause of the increase of the pressure loss.

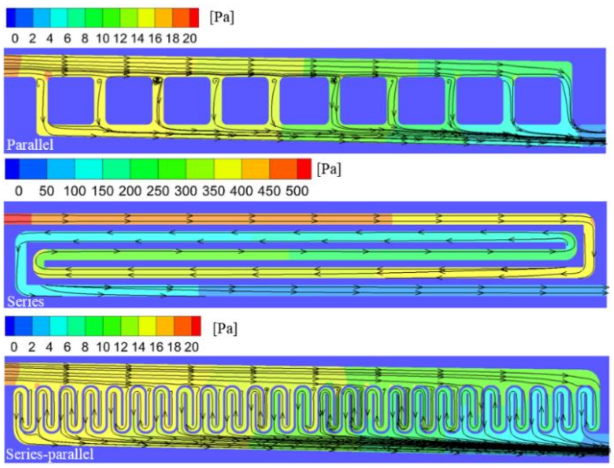

Figure 4. Mid surface pressure distribution (100W, 0.2 L/min)

The second reason is related to the configuration: For the "Series" case, the channel advances serially from the inlet to the outlet that results in cumulative pressure drop. The investigation of the pressure contours and the streamlines show that nearly the same flowrates within the cross channels has been achieved in "Series-parallel" case that has also positive influence on the low pressure loss. This uniformity is provided by changing shape of the inlet and exit manifolds and the width and number of the cross channels. On the other hand, uniform flow distribution is desired not only for low pressure drop but also to achieve uniform temperature distribution. Further investigations of the temperature field are made in the following subsection.

3.2 Temperature distributions

The temperature distribution corresponding to three configurations for the design flowrate obtained at the top surface adjacent to the heat source are shown in Fig. 5b. The contours show that the average, the minimum and the maximum temperature levels are higher in "Parallel" case. The exact values can be read from Table 2. Besides, Table 2 shows that the difference between maximum and minimum temperature is 6.60 K for "Parallel" case. This value is the highest one compared to the other two cases; and this is an unwanted situation that indicates non-uniformity. When Fig. 5 is examined further, one may expect to obtain the highest temperature region for each case at the lower right corner that is close to the exit of all the three channels. In that region, the cooling fluid is already heated up that is expected to decrease the cooling effect. This effect occurs for "Parallel and "Series-parallel" cases at low flowrates shown in Fig. 5a. Temperature contours for these cases show a gradual increase from left to the right since low temperature fluid enters to the domain from the left side. Isolines are almost vertical due to the relatively slower flow compared to the design flowrate, passing through vertical channels. On the other hand, "Series" case shows the maximum temperature at the central bottom region instead of the right side. This can be understood more easily by taking imaginary vertical cross sections at the left, centre and right sides of the cold plate in Fig. 1. The regions around left section (Section A) is already close to the inlet of the domain where the cooling fluid is still colder that helps better cooling. Also, due to the geometrical configuration, the working fluid in the vertical part of the channel corresponding to the Section C is not far away from the entrance thus it is also colder compared to the rest of the channel that makes spirals through the central regions. Besides, the left and the right sections (Section A and C) feels more mass flow due to the vertical passages of the channel around these positions, thus more cooling effect than central section plane (Section B). As a result, the temperature aggregates in the central section and the bottom of the Section B shows a higher temperature compared to other regions. For this "Series" case, the same effect can be seen at the design flowrate as well (Fig. 5b). When it comes to "Parallel" and "Series-parallel" cases, the design flowrate provides the flow passing almost equally through the vertical channels, however relatively higher velocity compared to low flowrates causes increased mass flow at the last channels. This results in a similar behavior with the "Series" case. Lower right corner of the "Series-parallel" and "Parallel" cases exposes to a large manifold with an increasing height from left to the right. That large manifold at the lower right corner provides more mass flow and thus better cooling compared to the centre of the bottom region. Similar phenomenon occurs at the upper left manifold as well. Finally, for the reasons explained above, for the design flowrate, the maximum temperature for all the three configurations occurs at the bottom central position.

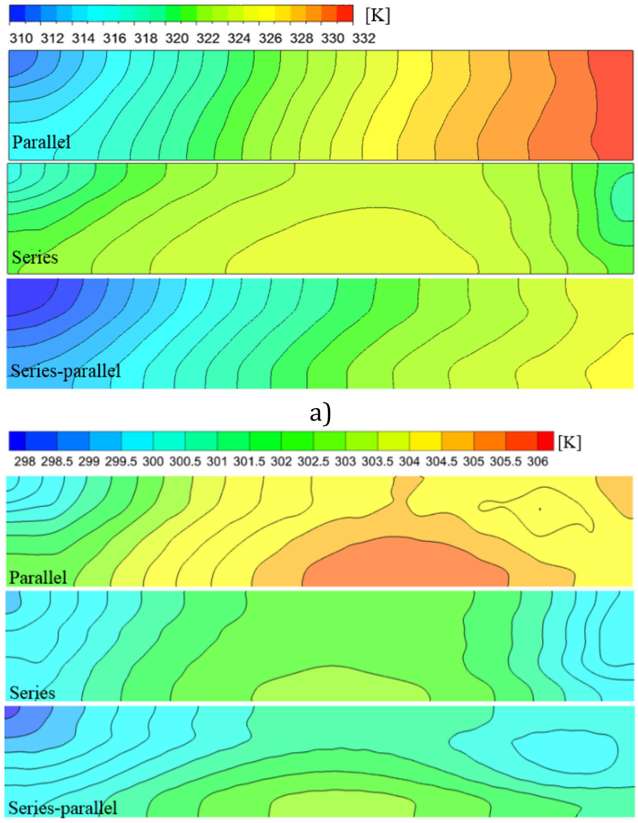

Figure 5. Top surface temperature distribution for a) low (100W, 0.05 L/min), b) design flowrate (100W, 0.2 L/min)

As explained before, a maximum value of 3-5 K is desired for battery cells. This goal is achieved for series case with 3.85 K and a small penalty nearly occurs in series-parallel case with 4.81 K. Though the values obtained in this study seems to reflect only the temperature distribution on the cold plate, one should keep in mind that higher uniformity of temperature in the cold plate results in higher uniformity of temperature inside the battery cell.

Table 2
Top surface temperature values (100W, 0.2 L/min)

Temperature (K)	Parallel	Series	Series-Parallel
Area Weighted Avg. Temp.	304.06	301.44	300.99
Surface Max. Temp.	305.97	302.69	302.69
Surface Min. Temp.	299.37	298.84	297.88
Surface ΔT	6.60	3.85	4.81

3.3 Performance charts

As mentioned before, for a better comparison of three cold plates, the simulations are extended to lower and higher flowrates. The performances of the cold plates are shown by thermal resistance and pressure drop vs. flowrate charts as these are the information generally provided in the literature and product catalogues. The corresponding charts are shown in Figure 6. Normalized thermal resistance that is preferred frequently by the manufacturers is used in the charts. This makes the resistance independent of the heat transfer area.

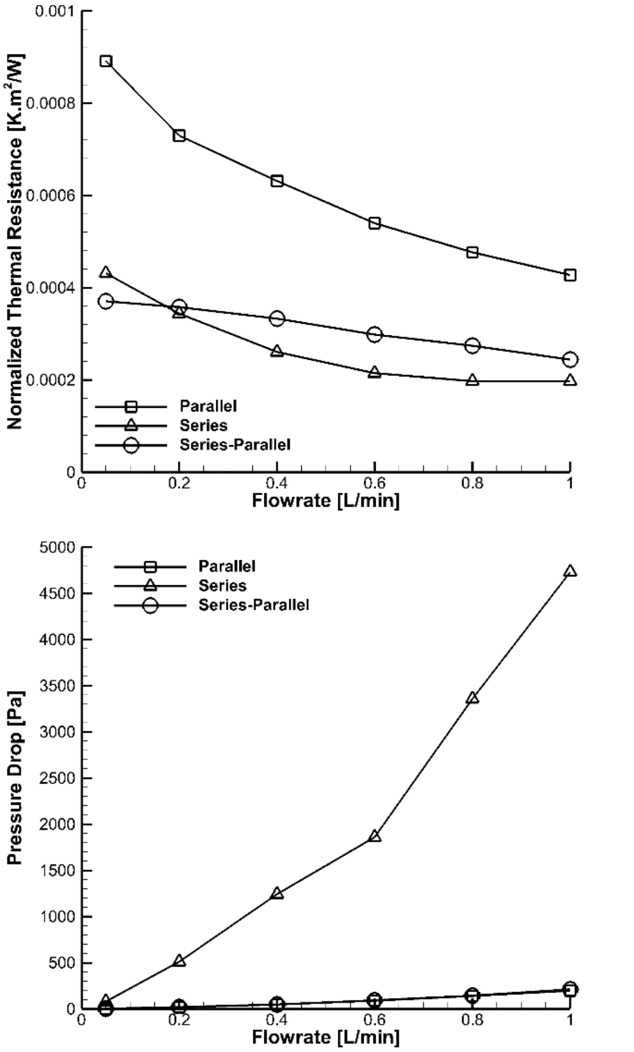

Figure 6. Normalized thermal resistance comparison and pressure drop comparisons

The formula used to calculate the normalized thermal resistance is shown in Equation (1).

$$R_n = (T_{top\_max} - T_{fluid_{out}})/\dot{Q}_{top} \qquad (1)$$

Figure 6 shows that normalized resistance decreases when flowrate increases for all the configurations. The trend and the inclinations of the curves of the parallel and series cases are similar except that the one of the series-parallel case is being more flat. The normalized thermal resistance of the "Parallel" case is the highest and the one of the "Series" is the lowest for high flowrates but these values approaches to each other and the grading is reversed for "Series" and "Series-parallel" cases at lower flowrates. The variation of the maximum temperature on the cold plate with the flowrate is shown in Fig. 7. Top surface maximum temperature values are very close in series and "Series-parallel" cases and are lower than the one of "Parallel" case. One should emphasize that the maximum temperature decreases with the flowrate. Although the detailed analyses are performed for the design flowrate in this study, this phenomenon shows that one should take into consideration all the performance map if flowrate is a parameter during real conditions. On the other hand, Figure 6 shows that pressure drops of "Parallel" and "Series-parallel" cases seem to be still comparable for all flowrates while the one of the "Series" case diverges further at high flowrates. This may be expected since pressure drop increase is proportional to square of velocity already mentioned in Section 3.1. On the other hand, the slope of the curve is much lower for the "Series-parallel" and "Parallel" cases. This is also expected since distribution and recollection of the parallel channels result in the same pressure loss through all parallel channels. This causes a low pressure drop compared to a long serial channel. When flowrate increases, the pressure drop difference between "Series" and "Series-parallel" or "Parallel" case shows an obvious divergence between the curves shown in Fig. 6. One should note that when Fig. 1 is investigated, in "Parallel" case, flow enters from a large manifold and the flow is divided to 10 horizontal channels. On the other hand, for "Series-parallel" case, this number increases to 25 with some spirals inside. These spirals increase the blockage to some degree by extending the length of the channel that increase pressure drop. However, increasing the number of the vertical channels compared to "Parallel" case decreases the blockage in front of the flow that provides more flow passing through the channels to the lower manifold. This compromise provides keeping the pressure drop of the "Series-parallel" case at the same order of magnitude with the "Parallel" one. Besides, one should remind that several design attempts are performed by taking number of the channels and the radius of curvature at the inlet of the vertical channels to obtain a low pressure loss, already mentioned in Section 2.1.

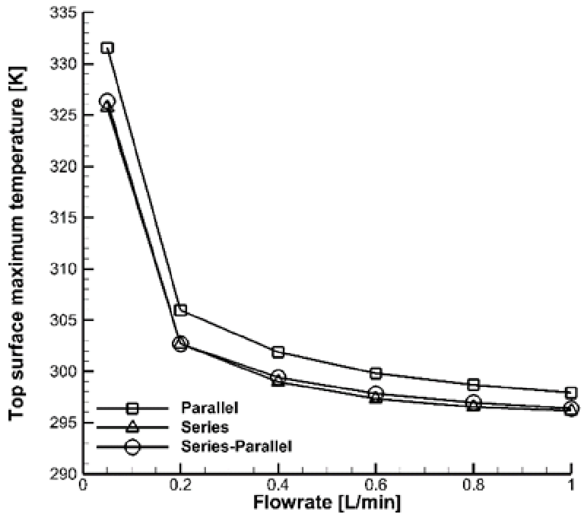

Figure 7. Comparison of top surface maximum temperature values

4. Conclusions

Three liquid cold plates having same outer dimensions but different internal flow configurations are designed and their performances are compared by means of CFD simulations. The following conclusions are observed:

1) The "Series" flow configuration shows lowest thermal resistance for the design flowrate that leads to low temperature on the surface but the pressure drop is much larger than the other cases.

2) The "Parallel" flow arrangement has highest thermal resistance for the design flowrate that leads to high temperature on the surface but the pressure drop is considerably lower compared to "Series" configuration case.

3) The "Series-parallel" flow arrangement has both low thermal resistance and low pressure drop for the design flowrate.

Series-parallel flow configuration can be a suitable compromise between the pressure drop and the heat transfer. It is possible to introduce further enhancements by designing cold plates with different series-parallel configurations.

Acknowledgment

Authors would like to thank TUBITAK Rail Transport Technologies Institute (RUTE) for the infrastructure used for this study.

Authorship Contributions

In this study; Ayhan Nazmi ILIKAN contributed in the fields of literature review, methodology, simulations, writing; Ahmet YAYLI, contributed in the fields of preparation of CAD models and literature review.

Conflict of Interest

The author declared no potential conflicts of interest with respect to the research, authorship, and/or publication of this article.

Nomenclature

$\dot{Q}$	heat transfer rate, [W]
R_n	normalized thermal resistance, [Km^2W^{-1}]
Re	Reynolds number (=velocity x characteristic length / kinematic viscosity), [–]
T	temperature, [K]
Subscripts	
N	normalized
To	top surface of the cold plate (adjacent to heat source)
top-max	maximum value at top surface of the cold plate (adjacent to heat source)
fluid-out	fluid property at outlet cross section from the cold plate

References

ANSYS FLUENT User's Guide 14.0. (2011). Modelling flows using sliding and dynamic meshes, ANSYS, Inc., 11, 610-612. Retrieved from https://www.afs.enea.it.

Chen, D., Jiang J., Kim, G., Yang, C., Pesaran, A. (2016). Comparison of different cooling methods for lithium ion battery cells, *Applied Thermal Engineering*, 94(1), 846-854. doi: https://doi.org/10.1016/j.applthermaleng.2015.10.015.

Datta, A.B., Majumdar, A.K. (1980). Flow distribution in parallel and reverse flow manifolds, *International Journal of Heat and Fluid Flow*, 2(4), 253-262. doi: https://doi.org/10.1016/0142-727X(80)90019-3.

Dincer, I., Hamut, H., Javani, N. (2017). Thermal management of electric vehicle battery systems, John Wiley and Sons Ltd., United Kingdom. Retrieved from https://www.wiley.com/en-us.

Haifeng, D., Ze-Chang, S., Xuezhe, W., Shugiang, Y. (2015). Design and simulation of liquid-cooling plates for thermal management of ev batteries, EVS28, Kintex, Korea, 1, pp. 1-7. Retrieved from https://www.evs28.org/

Jarrett, A. (2011). Multi-objective design optimization of electric vehicle battery cooling plates considering thermal and pressure objective functions, M. Sc. thesis, Queen's University, Ontario, Canada.

Jung, H.G., Jang, M.V., Hassoun, J., Sun, Y.K., Scrosati, B. (2011). A high-rate long-life Li4Ti5O12/Li[Ni0.45Co0.1Mn1.45]O4 lithium-ion battery, *Nature Communications*, 2, 516–520. doi: https://doi.org/10.1038/ncomms1527.

Kandlikar, S.G., Hayner II, C.N. (2009). Liquid cooled cold plates for industrial high-power electronic devices—thermal design and manufacturing considerations, *Heat Transfer Engineering*, 30(12), 918-930. doi: https://doi.org/10.1080/01457630902837343.

Khan, M.R., Swierczynski, M.J, Kaer, S.K. (2017). Towards an ultimate battery thermal management system: a review, *Batteries*, 3(1), 1-9. doi: https://doi.org/10.3390/batteries3010009.

Panchal, S., Mathewson, S., Fraser, R., Culham, R., Fowler M. (2015). Thermal management of lithium-ion pouch cell with indirect liquid cooling using dual cold plates approach, *SAE International Journal of Alternative Powertrains*, 4(2), 293-307. doi: https://doi.org/10.4271/2015-01-1184.

Rahman, M.M., Rahman, H.Y., Mahlia, T.M.I., Sheng, J.L.Y. (2016). Liquid cooled plate heat exchanger for battery cooling of an electric vehicle (EV), ICARET 2016, Selangor, Malaysia, 1, 1-4. doi: http://dx.doi.org/10.1088/1755-315/32/1/012053

Schöner, H.P., Ogborn, L.L. (1987). Fast battery to battery charge, *Journal of Power Sources*, 21, 91-103. doi: https://doi.org/10.1016/0378-7753(87)80040-X

Solovitz, S.A., Mainka, J. (2011). Manifold design for micro-channel cooling with uniform flow distribution, *ASME Journal of Fluids Engineering*, 133(5), 1-11. doi: https://doi.org/10.1115/1.4004089.

Teng, H., Yeow, K. (2012). Design of direct and indirect liquid cooling systems for high- capacity, high-power lithium-ion battery packs, *SAE International Journal of Alternative Powertrains*, 1(2), 525-536. doi: https://doi.org/10.4271/2012-01-2017.

Teng, H., Ma, Y., Yeow, K., Thelliez, M. (2011). Thermal characterization of a li-ion battery module cooled through aluminum heat-sink plates, *SAE International Journal of Passenger Cars—Mechanical Systems*, 4(3), 1331-1342. doi: https://doi.org/10.4271/2011-01-2248.

Warner, J. (2015). The handbook of lithium-ion battery pack design, chemistry, components, types and terminology, Elsevier, USA. Retrieved from https://www.elsevier.com.

Yeow, K., Teng, H., Thelliez, M., Tan, E. (2012). Thermal analysis of a li-ion battery system with indirect liquid cooling using finite element analysis approach, *SAE International Journal of Alternative Powertrains*, 1(1), 65-78. doi: https://doi.org/10.4271/2012-01-0331.

Yeow, K., Teng, H. (2013). Reducing temperature gradients in high-power, large-capacity lithium-ion cells through ultra-high thermal conductivity heat spreaders embedded in cooling plates for battery systems with indirect liquid cooling, SAE World Congress & Exhibition, Detroit, USA, 2013, 1(0234), 1-11. doi: https://doi.org/10.4271/2013-01-0234.